Journal of Alloys and Compounds 830 (2020) 154716

Contents lists available at ScienceDirect

Journal of Alloys and Compounds

journal homepage: http://www.elsevier.com/locate/jalcom

Impact of Al_2O_3 stress liner on two-dimensional SnS_2 nanosheet for photodetector application

Xinke Liu [a, 1], Xuanhua Deng [a], Xiaohua Li [a, 1], Hsien-Chin Chiu [b, c, *], Yuxuan Chen [d], V. Divakar Botcha [e], Min Wang [e], Wenjie Yu [f], Chia-Han Lin [b]

[a] College of Materials Science and Engineering, Chinese Engineering and Research Institute of Microelectronics, Shenzhen University, 3688 Nanhai Ave, Shenzhen, 518060, PR China
[b] Department of Electronic Engineering, Chang-Gung University, Taoyuan, 333, Taiwan
[c] Department of Radiation Oncology, Chang Gung Memorial Hospital, Taoyuan, 333, Taiwan
[d] State Key Laboratory of Luminescence and Applications, Changchun Institute of Optics, Fine Mechanics and Physics, Chinese Academy of Sciences, Changchun, 130033, PR China
[e] Photonics Center of Shenzhen University, 3688 Nanhai Ave, Shenzhen, 518060, PR China
[f] State Key Laboratory of Functional Materials for Informatics, Shanghai Institute of Microsystem and Information Technology, Chinese Academy of Sciences, 865 Changning Road, Shanghai, 200050, PR China

ARTICLE INFO

Article history:
Received 10 October 2019
Received in revised form
6 March 2020
Accepted 9 March 2020
Available online 10 March 2020

Keywords:
SnS_2
Al_2O_3 stress liner
Raman spectroscopy
Photodetector

ABSTRACT

Layered tin disulfide (SnS_2) nanosheets are gradually coming into people's vision as an emerging two-dimensional material for the potential application majority in optoelectronic field. We investigate a sample of ultra-thin SnS_2 nanosheets (~5 nm) on SiO_2/Si substrates and the photodetectors performance based on it with and without high-k ALD-Al_2O_3 stress liner. By means of temperature-dependent Raman spectroscopy, both a red-shift of Raman frequency from 313.1 cm^{-1} to 311.2 cm^{-1} as well as a reduction of the first order temperature coefficient from −0.01232 cm^{-1}/K to −0.00895 cm^{-1}/K are measured. For device, compared to SnS_2 photodetector, Al_2O_3/SnS_2 photodetector shows enhancement with 7-times light current, 10-times responsivity, 25%-off rising time and 70%-off falling time under 365 nm illumination. The phenomena can be rationalized by factors that the SnS_2 sample suffers a tensile strain and passivation effect exerted by capped Al_2O_3 layer. Meanwhile, the first principle calculations assist the study from an angle of verification. The analogue stress treatment operated in this work improves the properties of SnS_2 and enhances the performances of SnS_2-based photodetectors, aiming at expanding the thin-film materials applications in optoelectronic devices.

1. Introduction

With graphene initially developed, two-dimension (2D) materials equipped with unique mechanical, thermal, electronic and photonic properties attracted considerable interest in the fields of materials science, condensed matter physics, optoelectronics and nanotechnology [1]. However, the role of zero-overlap semimetal embarrassed graphene application, so the perspective was shifted to form composite heterostructures or seek other 2D materials intrinsically with bandgap, instead of tortuously opening a bandgap [2–4]. Transition metal dichalcogenides (TMDCs), the class of semiconductors in the chemical form of MX_2, where M (M = Mo, W, Nb, Sn) and X (X = S, Se, Te) correspond to transition metal and chalcogen, entered people's sight. In particular, MoS_2, WS_2, $MoSe_2$ and WSe_2 with controllable bandgaps ranging from 0.4 eV to 2.3 eV, aroused tremendous attention for applications in microelectronics and optoelectronics [5–9]. Tin disulfide (SnS_2), a group IV–VI compound among TMDCs, is consisted of most earth-abundant and environmentally friendly elements, crystallizing as a layered CdI_2-type structure, in which the Sn atoms are sandwiched by two layers of S atoms. Atoms are hexagonally connected by internal covalent bonding, while three-atom-thick layers are stacked together by weak van der Waals interactions, with lattice constants of a = b = 0.365 nm, c = 0.589 nm SnS_2 thin films are mostly prepared by spray pyrolytic deposition [10], liquid phase exfoliation

* Corresponding author. Department of Radiation Oncology, Chang Gung Memorial Hospital, Taoyuan, 333, Taiwan.
E-mail address: hcchiu@mail.cgu.edu.tw (H.-C. Chiu).
[1] These authors contributed equally to this work.

https://doi.org/10.1016/j.jallcom.2020.154716
0925-8388/

[11], micromechanical exfoliation [12], hydrothermal [13] and chemical vapor deposition [14,15] methods and have realized large-scale synthesis [15–17]. Differing from MoS_2, which shows the transition from an indirect bandgap to a direct one with decreased number of layers, SnS_2 maintains the indirect bandgap of about 2.0–2.6 eV in all kinds of forms, including monolayer, bilayer and bulk. The mechanism of correlation between bandgap and number of layers is still unclear [15,18], but a direct bandgap can be induced by effect of biaxial tensile strain or a thermally activated pathway [19,20]. According to the reports, the measured carrier mobilities in monolayer SnS_2 devices are 50 and 230 $cm^2V^{-1}s^{-1}$, and continuously rise with increasing thickness of the channel in SnS_2 field-effect transistors (FETs); meanwhile, the high on/off current ratios (I_{on}/I_{off}) can reach up to 10^6-10^8 [12,21]. In addition, the current response time of thin crystal arrays of SnS_2 photodetector with seed engineering can be as short as ~5 μs[14]; the ultrahigh sensitivity ($>10^6$ AW^{-1}), detectivity ($>10^{12}$-10^{13} Jones), as well as responsivity (244 AW^{-1}) were demonstrated in photodetectors based on SnS_2 nanosheet/PbS CQD hybrid and WSe_2/SnS_2 vdW heterostructure [22,23]. Besides those applications for FETs and photodetectors in microelectronic and optoelectronic fields, the enormous potential of 2D SnS_2 is also offered diversified material platforms for gas sensing [24], energy conversion and energy storage, such as water splitting [25] and photocatalyst in SnS_2-based 2D/1D or 2D/2D heterostructures with TiO_2, SnO_2, g-C_3N_4 and other nanomaterials [13,26,27]. Particularly as anode in batteries, considering the relatively poor conductivity and experiences large volume change during electrode reactions, SnS_2 was developed by hybridization with graphene, reduced graphene oxide (rGO) or other alternative conductive nanomaterials and applied in lithium ion and sodium ion batteries [28–33], to solve the electrode pulverization problem and further enhance the cycling performance.

In this paper, we report the light-induced electric properties of photodetectors based on ultra-thin layered SnS_2 nanosheets with and without a ~3 nm Al_2O_3 stress liner. The mechanically-exfoliated SnS_2 sample was prepared upon SiO_2/Si substrates and capped a high-k oxide layer via atomic layer deposition (ALD). Besides, we investigated the scattering variation from single material to composites using typical and temperature-dependent Raman spectra measurements. As a result, the processed Al_2O_3/SnS_2 photodetector behaves an advanced performance in photoresponse, and we attribute the enhancement to the additional Al_2O_3 layer with its applied tensile strain and passivation effect. Last, first principle calculations were carried out to verify our experiments and reasonings. The similar operation given can be reproduced between other layered semiconductor and high-k dielectric materials to enhance properties and extend applications in optoelectronics devices profoundly.

2. Experiment

The layered SnS_2 was prepared by standard mechanical exfoliation method from SnS_2 flakes, and then transferred onto the silicon substrate, whose surface was superficially oxidized into 300-nm-thick silicon oxide. Subsequently, we fabricated SnS_2 photodetector, using electron beam lithography (EBL) system (Raith EBPG 5150, PIONEER Two) to define the electrode patterns as well as thermal evaporation equipment (ASB-EPI-C6) to deposit Ti/Au (10 nm/100 nm) metal stack. Later, the SnS_2 nanosheets was covered with a 3-nm-thick Al_2O_3 stress liner grown from the precursors of trimethyl-aluminum (TMA1) and water at 300 °C through the ALD process. Fig. 1(a) shows the structure model schematic diagram of the as-prepared SnS_2-based photodetectors, and the inset is the corresponding optical microscope image in looking-down perspective.

3. Results and discussion

The exfoliated SnS_2 nanosheets transferred on SiO_2/Si substrate were situated and probed surface features in detail by atomic force microscopy (AFM, Bruker Dimension ICON) via the tapping mode. Fig. 1(b) is the height profile across the edge of the sample, where the thickness of the nanosheets is ~5 nm; the inset is an enlarged AFM image, in which the morphology of selected sample can be observed as a clear, smooth and graphic-regular film with distinct boundaries and uniform color. According to the thickness of monolayer (0.59 nm) reported in previous research, the nanosheets can be inferred as a stack of about 8–9 SnS_2 layers.

Raman spectroscopy is a nondestructive technique to analyze the structure, component, morphology and properties of materials, especially the ultrathin 2D materials for their typically changing film performance related to layer number. A typical Raman study was carried out in a confocal microprobe system at room temperature. A green laser source was excited at 514 nm and below 0.25 mW to avoid Raman shift introduced by local laser heating. Fig. 1(c) shows the typical comparative Raman spectra of the original SnS_2 nanosheets and the Al_2O_3/SnS_2 heterostructure after ALD process. Obviously, the Raman peak of the intrinsic SnS_2 nanosheets correspond to the vibrational A_{1g} mode was intensely positioned at 313.1 cm^{-1}, similar to previous researches, indicating that the polytype is 4H-SnS_2 crystals. Moreover, most described another feeblish doublet caused by E-mode at about 200 cm^{-1} and 214 cm^{-1} in 4H-SnS_2 bulk [16], but it disappeared in our work. The cause might be the reduction in in-plane scattering center along with the decrease of the thickness down to the nanometer scale, which forbade the relatively weaker peaks due to the energy degeneracy or Raman selection rules. In contrast with the intrinsic SnS_2 nanosheets, the Al_2O_3/SnS_2 heterostructure shows a down-shift of Raman frequency at 311.2 cm^{-1}. The red-shifts are attributed to the tension introduced by the stress liner and the changes of bond lengths and angles in lattice structure. It is believed the major contribution came from the decoration of Al_2O_3 rather than from the heat process of ALD treatment, because two samples show similar mode peak. The existence of Al_2O_3 in SnS_2/Al_2O_3 did not bring neither a compositional evolution nor a microstructural change on SnS_2. Besides, the Raman intensity of SnS_2/Al_2O_3 is proximately closed to that of SnS_2, even weaker, so, the development of crystallinity like in annealing process did not take place. On the other hand, the high and stable crystallinity of SnS_2 exfoliated from flaks, as well as, the controlled time condition of ALD process (150 s) are insufficient for recrystallization.

As we know, vibrational frequency has a high sensitivity to temperature variation, so Raman thermography is popularly used to study the thermal properties, such as thermal stability and thermal conductivity, of layered nanomaterials. And it provides a perspective for the further understanding of crystal structure, electron–phonon interaction and carrier transportation, which paly dominant roles in electronic mechanisms of semiconductors. A temperature-dependent Raman spectroscopy study was taken with the same excited laser above. The wide variation range of temperature was limited from room temperature (300 K) to 540 K and a 5-min waiting was needed after every warming for the sake of thermal stabilization. Fig. 2(a) and (b) show the temperature-dependent Raman spectra of layered SnS_2 nanosheets with and without Al_2O_3 stress liner respectively, in the range from 300 to 540 K. The similarity between two graphs is a Raman red-shift as temperature rises; but for comparison, the extent of red-shift is different. This could be more intuitively observed in Fig. 2(c). By means of Gauss and linear fitting, the relation between Raman frequency and temperature can be described as a linear function: $\omega = \omega_0 + \chi_T \Delta T$, where ω_0 is the Raman frequency at room

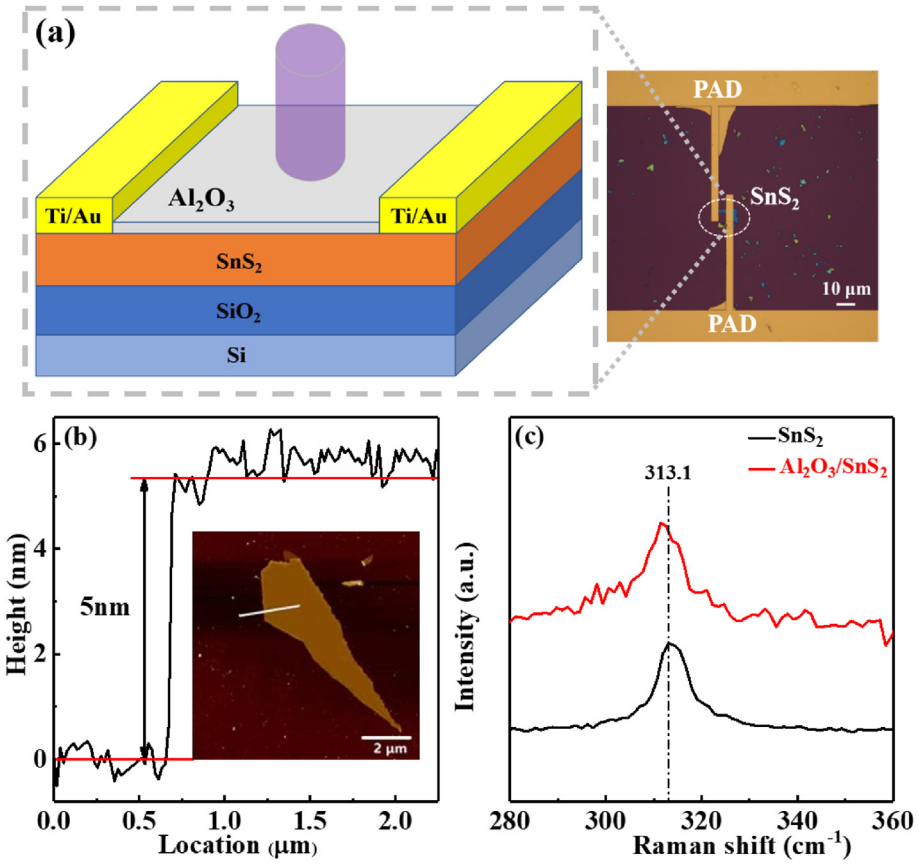

Fig. 1. (a) Structure model schematic diagram of the SnS_2-based photodetector and the optical microscope image; (b) The height profile of ultrathin SnS_2 nanosheets along the auxiliary line in inset (corresponding typical AFM image); (c) Raman spectra of SnS_2 and Al_2O_3/SnS_2 at room temperature.

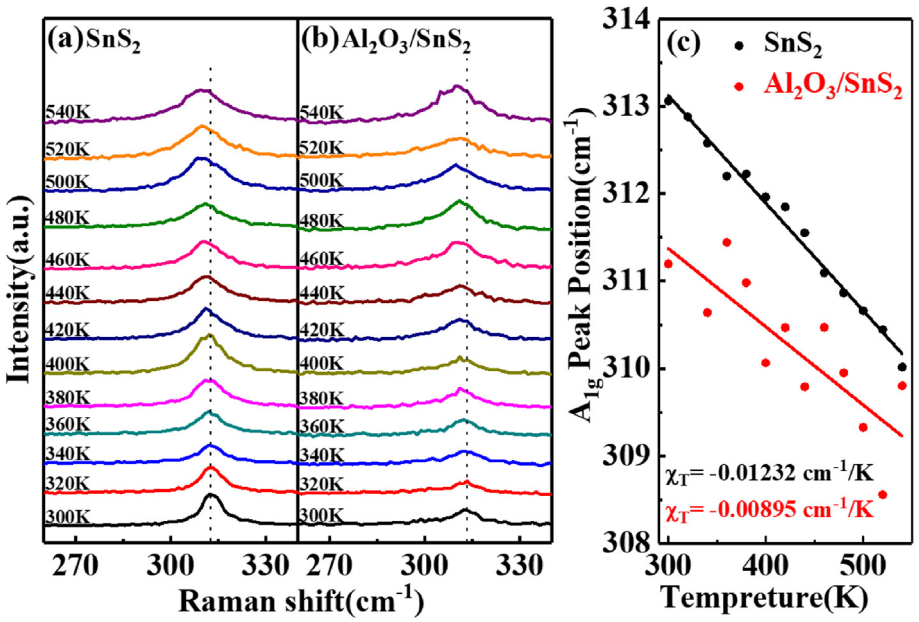

Fig. 2. Variable temperature Raman spectra of (a) SnS_2 and (b) Al_2O_3/SnS_2 samples in the range of 300–500 K; (c) A_{1g} mode Raman peak position shifts as a function of temperature via Gauss and linear fits.

temperature, χ_T is the first-order temperature coefficient, and ΔT is the temperature difference to room temperature. With the unified warming process, the reducing rate of Al_2O_3/SnS_2 Raman peak position was slower. Similar linear phenomenon agrees with several previous reports in 2D materials, such as graphene and other TMDCs [34,35]. Statistics shows that the χ_T value of SnS_2/

Al_2O_3 sample(-0.00895 cm^{-1}/K) was numerically smaller than the corresponding value of SnS_2 sample (−0.01232 cm^{-1}/K). As we known, the temperature-dependent Raman shift is attributed to anharmonicity, which is related to the potential energy introduced by phonon-phonon interactions [34]. The result of smaller slope indicates a progressive thermal stability in the decorated sample, due to different thermal expansion coefficients (TEC) between SnS_2 and Al_2O_3. In the SnS_2/Al_2O_3 sample, the in-plane thermal expansion coefficient of SnS_2 is about 10.0×10^{-5}/K, which is much larger than that of Al_2O_3 about 7.5×10^{-6}/K. As the temperature rises (falls), the SnS_2 layer expands (contracts) larger than the Al_2O_3. Equivalently, with temperature varies, this TEC mismatch would hinder the intrinsic thermal expansion or contraction of SnS_2 lattice, which induce a biaxial compressive or tensile strain; furthermore, a relative slipping would occur at the interface if the strain increases significantly over the weak van der Waals force. In our work, the tensile strain effectively affected the vibrations of the lattice and be reflected in the Raman frequency as a reduction of the red shift. The result correlates well with the Raman spectra results of other 2D materials with substrates supported or oxide passivation layer coated, where excitation laser power brings about strong thermal effects [36]. We also find the experiment counting points of Al_2O_3/SnS_2 are more divergent, in other words, the data statistical variance and standard deviation of peak position are higher. The distortion away from an intrinsic linear dependence was reported from the interaction between 2D material and substrates, but we are inclined that the bond is too weak to modulate a few-layer SnS_2 nanosheets. Our judgement depends on a relevant Raman research, which concluded that the Raman spectra of monolayer and bilayer SnS_2 films are externally modulated by substrates, while the SnS_2 flakes over four layers are intrinsically analogous with bulks. Therefore, the dispersion of data points may be experimentally introduced by the slight change of focused laser spot or the extra attenuation of excited laser power from cold-hot window during the measurements.

Here, we further fabricated a photodetector based on SnS_2 nanosheets and then carried out its light-induced electric properties measurements using a Keysight B1500A semiconductor device analyzer at room temperature in ambient environments. Fig. 3(a) shows the current-voltage (I-V) characteristics of SnS_2 photodetector in dark and exposed to light of various laser wavelengths (365 nm,460 nm and 660 nm). The I-V curve approximate achieved a linear increase with voltage ranging from −5 V to 5 V, indicating a well ohmic contact between SnS_2 and electrodes. According to the materials bandgap (~2.0—2.6 eV), the cut-off wavelength can be calculated as ~477-620 nm, between the pre-set 460 nm and 660 nm wavelengths. So the curve at 660 nm wavelength can be neglected. And following photoresponse properties were measured under 365 nm illumination for its highest response. By contrast, at applied voltage of 5 V, the illumination current of Al_2O_3/SnS_2 photodetector (5.05×10^2 nA) is 7 times stronger than that of SnS_2 photodetector. The photocurrent, defined as the difference value between illumination current and dark current ($I_{ph} = I_{illuminated} - I_{dark}$), improves remarkably by an order of magnitude. Either does the responsivity (R) shown in Fig. 3(b). The calculated maximum responsivity in stress liner device is up to 896.7 A/W (with the power density of 11.92 mW/cm^2), the photo-gain (G) increases to 3052, and the I_{on}/I_{off} ratio is about 21. For further study on noise performance, noise equivalent power (NEP) and normalized detectivity (D*) are estimated to 9.703×10^{-17} W and 2.186×10^{14} cm $Hz^{0.5}W^{-1}$, respectively. The calculation method in details can be referred to the previous work [37]. Compared with previous results, our device is good at R and G but embarrassed in I_{on}/I_{off}, NEP and D* [14,16,17]. The improvement of electrical conductivity and responsivity, on one hand, can be attributed to the interface charges existed at the interfacial between SnS_2 layers and Al_2O_3 layers, which cause electron-phonon interactions; on the other hand, it may be due to the tensile strain stressed by Al_2O_3 with different TEC, which changed the bond lengths and angles of lattice structures, and thus affected the bandgap of SnS_2. However, the stress liner also seriously influenced the dark current and noise characteristics by same way. So that is the next project for us to lower the dark current and noise to strive for further improvement of materials and device performances. Here, In order to enlarge the optoelectronic application, we further explored the time-resolved photoresponse of both SnS_2 and Al_2O_3/SnS_2 photodetectors with a bias voltage of 5 V under 365 nm illumination, and then recorded the rise and decay curve at a photo-switch period of 10 s, as shown in Fig. 3(c) and (d), respectively. The regular shifts of plot, that the curve rises up to a high level as on-state under illumination and returns down to low level as off-state in dark, convey that the device is under the satisfactory performance of photostability and repeatability. Another critical parameter to evaluate the performance of photodetector is the response time. The inset in Fig. 3(d) is a single period intercepted in the rise and decay behavior of Al_2O_3/SnS_2 photodetector. With laser switched on, the photocurrent took a rising time of 2.91 s to reach 90% of the peak value; meanwhile, with laser switched off, it reduced down to 10% in a falling time of 2.29 s. The results are making pronounced progress than the corresponding time values of previous SnS_2 photodetector. Because the weak illumination current causes photocurrent to appear a relatively strong fluctuation after cancelling the light condition, the curve is difficult to be expressed by plotting. Instead, through approximation and fitting treatments, the rising time and falling time in SnS_2 photodetector is measured as about 3.85 s and 7.67 s, respectively. In other words, the ALD treatment shortens rising time by 25% and falling time by 70%, respectively. It reveals that air adsorption and perturbation badly affect the photoconduction, especially in decay processes for ultra-thin 2D semiconductor materials with large specific surface area. More specifically, the air, such as oxygen, adsorbed onto the surface of n-type SnS_2 nanosheets will create an electronic depletion layer trap the electrons and reduce the carrier concentration in dark condition. While in illuminating environments, the holes separated from photon-generated carriers will migrate and recombine with the trapped electrons and then release the oxygen. Besides, the surface trap states could prolong the lifetime of photogenerated carriers in similar principle as well. On the macro perspective, longer carrier lifetime improves responsivity but slow down the response rate. In our work, the processed Al_2O_3 capping layer avoids the photooxidation and photodegradation under ambient conditions. The SnS_2 photodetector with Al_2O_3 stress liner gains overall advantages against the homologous SnS_2 photodetector in light-induced electric properties, including photoresponse, responsivity, as well as photo-switch effect.

First-principles calculations are carried out using Cambridge Sequential Total Energy Package (CASTEP). Instead of standard density functional theory (DFT), the Perdew-Burke-Ernzerhof (PBE) generalized gradient approximation (GGA) density functional is used to calculate the ground state lattice parameters and band structure of SnS_2 in condition of these long-range dispersive interactions [38]. Meanwhile, projector augmented-wave method (PAW) is in consideration for ion-electron interactions [39]. A cut-off energy of 400 eV and a Γ-centered Monkhorst-Pack k-mesh of $4 \times 4 \times 1$ grid are employed in the sampling the Brillouin zone in structure optimization and total energy calculation [40]. The cut-off energy and k-point grid are chosen as such that the maximum force is less than 0.003 eV/nm and the stress is converged to within 0.05 GPa on each atom. Fig. 4(a)—(d) image the results of the few-layer SnS_2 band structure calculation with tensile strain in the

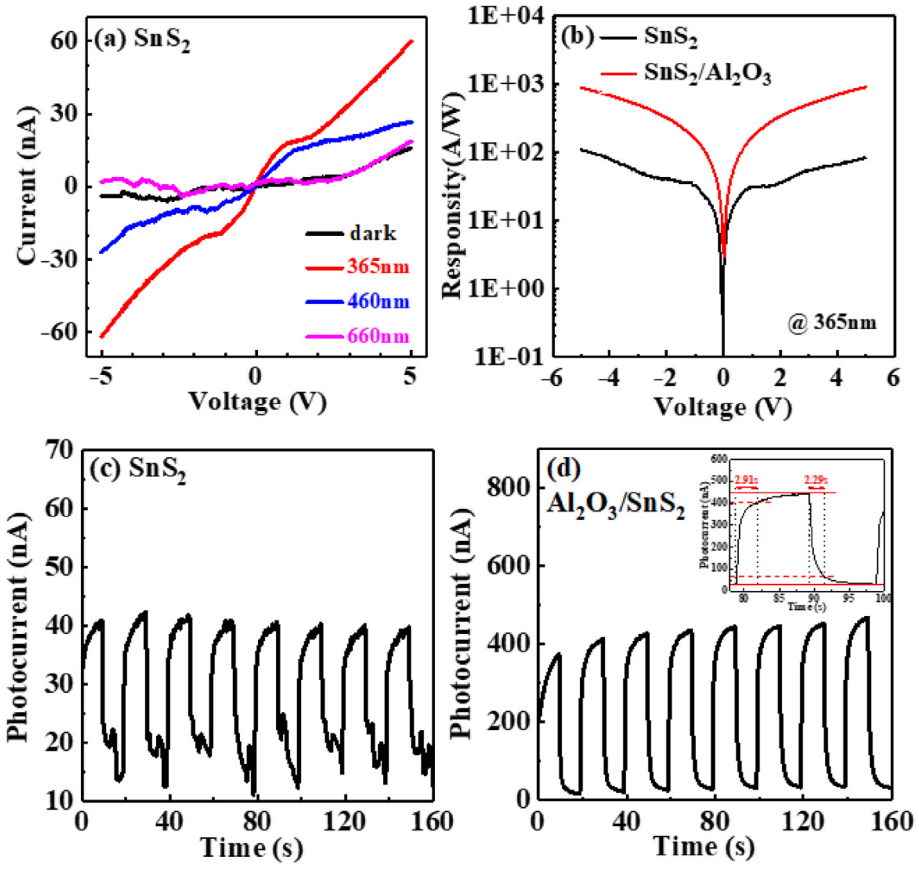

Fig. 3. (a) I-V characteristics of SnS_2 photodetector in dark and under illumination of various wavelengths; (b) Responsivity of SnS_2 and Al_2O_3/SnS_2 photodetectors under 365 nm illumination; (c)–(d) Time-resolved curve of the SnS_2 and Al_2O_3/SnS_2 photodetectors with the voltage of 5 V under 365 nm illumination, respectively; inset of (d): the corresponding rise time and decay time.

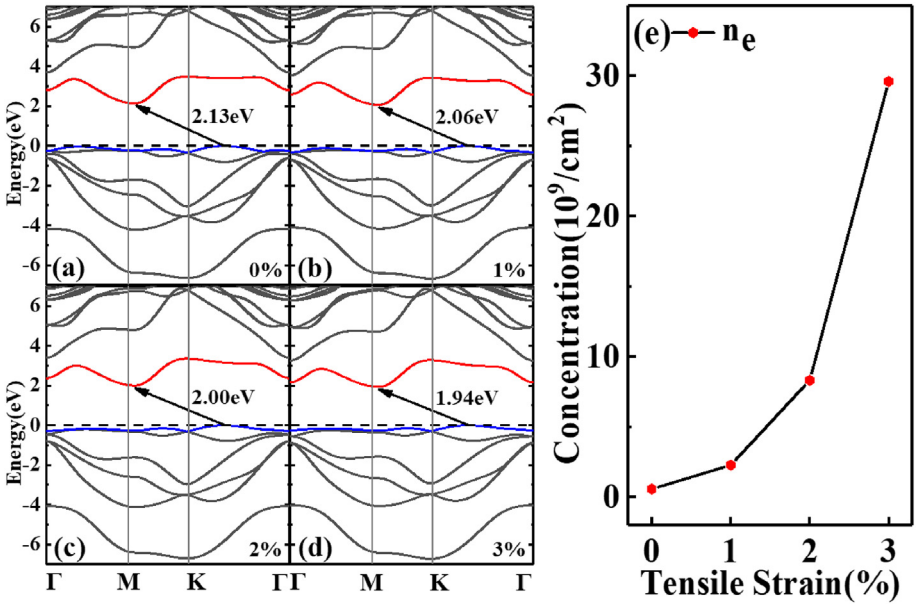

Fig. 4. The simulation on band structures for ~5 nm SnS_2 with (a) 0%, (b) 1%, (c) 2% and (d) 3% tensile strain; (e) the variation of the corresponding electron concentration with various tensile strain.

range from 0% to 3%. As the increasing of biaxial tensile strain with changing lattice constant, the bandgap reduces continually from 2.13 eV to 1.94 eV. The underlying principle is that strain weakens the interplay of in-plane orbits and eventually changes the properties of dispersion and valence band edges, resulting in changes in band gaps. Accordingly, the effective mass of carriers is affected by

$m^* = \hbar^2 \Big/ \left(\frac{\partial^2 E}{\partial k^2}\right)$, and the electron concentration (n_e) is estimated as:

$$n_e = 2\left(\frac{k_B T}{2\pi\hbar^2}\right)^{\frac{3}{2}} (m_e m_h)^{\frac{3}{4}} \exp\left(-E_g / 2k_B T\right),$$

where k_B is Boltzmann constant, T is the temperature, $\hbar = h/2\pi$, h is Planck constant, m_e (m_h) is mass of electron (hole), and E_g is bandgap. As shown in Fig. 4(e), n_e is increasingly intense with stronger tensile strain. As a consequence, the thermal conductivity is dominated by both effective mass of carriers and electron concentration and described in formula: [41],

$$k_e = \pi^2 T k_B^2 n_e \Big/ 3 m_e^* v_e$$

where T is the temperature, k_B is the Boltzmann constant, n_e is the electron concentration, m_e* is the effective mass of electron and v_e is the total effective electron collision frequency. Simulation proves that the enhancement of thermal conductivity is investigated mainly in electron concentration, which rise for narrower bandgap and originally on account of introduced tensile strain. Therefore, the theory is properly correlated to the Raman spectroscopy experiment.

4. Conclusions

In summary, ultra-thin layered SnS_2 nanosheets were mechanically exfoliated on SiO_2/Si substrates, covered with a ~3 nm ALD-Al_2O_3 layer, and fabricated as a photodetector. Through the capping process of the oxide, the measured Raman peak position of A_{1g} vibration mode in SnS_2 exists a red-shift from 313.1 cm^{-1} to 311.2 cm^{-1} at room temperature, indicating the structure change of material; in temperature-dependent Raman spectroscopy measurements, the first order temperature coefficient is found numerically decreasing from −0.01232 cm^{-1}/K to −0.00895 cm^{-1}/K, demonstrating the improved thermal stability. Under 365 nm illumination, the further fabricated Al_2O_3/SnS_2 photodetector shows a 7-times larger current, a 10-times improved responsivity (896.7 A/W) and a saving of 25% rising time and 70% falling time. We achieved the enhancements due to the increasing concentration of carriers introduced by tensile strain, electron-phono interactions, and passivation effect generated at the interface of Al_2O_3/SnS_2. The explanation is eventually proven by theoretical simulation.

Declaration of competing interest

We confirm that there are no known conflicts of interest associated with this publication and there has been no significant financial support for this work that could have influenced its outcome.

CRediT authorship contribution statement

Xinke Liu: Supervision. **Xuanhua Deng:** Data curation, Formal analysis. **Xiaohua Li:** Supervision. **Hsien-Chin Chiu:** Supervision. **Yuxuan Chen:** Data curation, Formal analysis. **V. Divakar Botcha:** Methodology. **Min Wang:** Data curation, Formal analysis. **Wenjie Yu:** Conceptualization, Investigation. **Chia-Han Lin:** Conceptualization, Investigation.

Acknowledgments

This work is financially supported by National Natural Science Foundation of China (61674161), Guangdong Province Key Research and Development Plan (2019B010138002), National Science and Technology Major Project of the Ministry of Science and Technology of China (2017ZX01032101-002), and the Open Project of State Key Laboratory of Functional Materials for Informatic. The authors wish to acknowledge device fabrication process in the Photonics Center of Shenzhen University.

References

[1] S. Cakmakyapan, P.K. Lu, A. Navabi, M. Jarrahi, Gold-patched graphene nanostripes for high-responsivity and ultrafast photodetection from the visible to infrared regime, Light Sci. Appl. 7 (2018) 20.
[2] W. Strek, B. Cichy, L. Radosinski, P. Gluchowski, L. Marciniak, M. Lukaszewicz, D. Hreniak, Laser-induced white-light emission from graphene ceramics—opening a band gap in graphene, Light Sci. Appl. 4 (2015) 237.
[3] C. Xie, Y. Wang, Z.-X. Zhang, D. Wang, L.-B. Luo, Graphene/semiconductor hybrid heterostructures for optoelectronic device applications, Nano Today 19 (2018) 41–83.
[4] C. Xie, C. Mak, X. Tao, F. Yan, Photodetectors based on two-dimensional layered materials beyond graphene, Adv. Funct. Mater. 27 (2017), 1603886.
[5] J. Yang, Z. Wang, F. Wang, R. Xu, J. Tao, S. Zhang, Q. Qin, B. Luther-Davies, C. Jagadish, Z. Yu, Y. Lu, Atomically thin optical lenses and gratings, Light Sci. Appl. 5 (2016), 16046.
[6] S. Jo, N. Ubrig, H. Berger, A.B. Kuzmenko, A.F. Morpurgo, Mono- and bilayer WS2 light-emitting transistors, Nano Lett. 14 (2014) 2019–2025.
[7] J. Xiao, Z. Ye, Y. Wang, H. Zhu, Y. Wang, X. Zhang, Nonlinear optical selection rule based on valley-exciton locking in monolayer ws2, Light Sci. Appl. 4 (2015) 366.
[8] B. Chamlagain, Q. Li, N.J. Ghimire, H.J. Chuang, M.M. Perera, H. Tu, Y. Xu, M. Pan, D. Xiao, J. Yan, D. Mandrus, Z. Zhou, Mobility improvement and temperature dependence in MoSe2 field-effect transistors on parylene-C substrate, ACS Nano 8 (2014) 5079–5088.
[9] H.J. Chuang, X. Tan, N.J. Ghimire, M.M. Perera, B. Chamlagain, M.M. Cheng, J. Yan, D. Mandrus, D. Tomanek, Z. Zhou, High mobility WSe2 p- and n-type field-effect transistors contacted by highly doped graphene for low-resistance contacts, Nano Lett. 14 (2014) 3594–3601.
[10] B. Thangaraju, P. Kaliannan, Spray pyrolytic deposition and characterization of SnS and SnS2 thin films, J. Phys. D Appl. Phys. 33 (2000) 1054–1059.
[11] J.F. Shen, Y.M. He, J.J. Wu, C.T. Gao, K. Keyshar, X. Zhang, Y.C. Yang, M.X. Ye, R. Vajtai, J. Lou, P.M. Ajayan, Liquid phase exfoliation of two-dimensional materials by directly probing and matching surface tension components, Nano Lett. 15 (2015) 5449–5454.
[12] H.S. Song, S.L. Li, L. Gao, Y. Xu, K. Ueno, J. Tang, Y.B. Cheng, K. Tsukagoshi, High-performance top-gated monolayer SnS2 field-effect transistors and their integrated logic circuits, Nanoscale 5 (2013) 9666–9670.
[13] Y.C. Zhang, L. Yao, G.S. Zhang, D.D. Dionysiou, J. Li, X.H. Du, One-step hydrothermal synthesis of high-performance visible-light-driven SnS2/SnO2 nanoheterojunction photocatalyst for the reduction of aqueous Cr(VI), Appl. Catal. B Environ. 144 (2014) 730–738.
[14] G.X. Su, V.G. Hadjiev, P.E. Loya, J. Zhang, S.D. Lei, S. Maharjan, P. Dong, P.M. Ajayan, J. Lou, H.B. Peng, Chemical vapor deposition of thin crystals of layered semiconductor SnS2 for fast photodetection application, Nano Lett. 15 (2015) 506–513.
[15] G. Ye, Y. Gong, S. Lei, Y. He, B. Li, X. Zhang, Z. Jin, L. Dong, J. Lou, R. Vajtai, W. Zhou, P.M. Ajayan, Synthesis of large-scale atomic-layer SnS2 through chemical vapor deposition, Nano Res. 10 (2017) 2386–2394.
[16] X. Zhou, Q. Zhang, L. Gan, H. Li, T. Zhai, Large-size growth of ultrathin SnS2 nanosheets and high performance for phototransistors, Adv. Funct. Mater. 26 (2016) 4405–4413.
[17] J. Xia, D. Zhu, L. Wang, B. Huang, X. Huang, X.-M. Meng, Large-scale growth of two-dimensional SnS2 crystals driven by screw dislocations and application to photodetectors, Adv. Funct. Mater. 25 (2015) 4255–4261.
[18] J.M. Gonzalez, I.I. Oleynik, Layer-dependent properties of SnS2 and SnSe2 two-dimensional materials, Phys. Rev. B 94 (2016), 125443.
[19] B. Ram, A.K. Singh, Strain-induced indirect-to-direct band-gap transition in bulk SnS2, Phys. Rev. B 95 (2017), 075134.
[20] P. Bhaskar, A.W. Achtstein, M.J.W. Vermeulen, L.D.A. Siebbeles, Unconventional thermally activated indirect to direct radiative recombination of electrons and holes in tin disulfide two-dimensional van der Waals material, J. Phys. Chem. C 123 (2019) 11968–11973.
[21] Y. Huang, E. Sutter, J.T. Sadowski, M. Cotlet, O.L.A. Monti, D.A. Racke, M.R. Neupane, D. Wickramaratne, R.K. Lake, B.A. Parkinson, P. Sutter, Tin disulfide-an emerging layered metal dichalcogenide semiconductor: materials properties and device characteristics, ACS Nano 8 (2014) 10743–10755.
[22] L. Gao, C. Chen, K. Zeng, C. Ge, D. Yang, H. Song, J. Tang, Broadband, sensitive and spectrally distinctive SnS2 nanosheet/PbS colloidal quantum dot hybrid photodetector, Light, Sci. App. 5 (2016), e16126.
[23] X. Zhou, X. Hu, S. Zhou, H. Song, Q. Zhang, L. Pi, L. Li, H. Li, J. Lü, T. Zhai, Tunneling diode based on WSe2/SnS2 heterostructure incorporating high detectivity and responsivity, Adv. Mater. 30 (2018), 1703286.
[24] J.Z. Ou, W.Y. Ge, B. Carey, T. Daeneke, A. Rotbart, W. Shan, Y.C. Wang, Z.Q. Fu,

A.F. Chrimes, W. Wiodarski, S.P. Russo, Y.X. Li, K. Kalantar-zadeh, Physisorption-based charge transfer in two-dimensional SnS2 for selective and reversible NO2 gas sensing, ACS Nano 9 (2015) 10313–10323.
[25] Y.F. Sun, H. Cheng, S. Gao, Z.H. Sun, Q.H. Liu, Q. Liu, F.C. Lei, T. Yao, J.F. He, S.Q. Wei, Y. Xie, Freestanding tin disulfide single-layers realizing efficient visible-light water splitting, Angew. Chem. Int. Ed. 51 (2012) 8727–8731.
[26] Z.Y. Zhang, C.L. Shao, X.H. Li, Y.Y. Sun, M.Y. Zhang, J.B. Mu, P. Zhang, Z.C. Guo, Y.C. Liu, Hierarchical assembly of ultrathin hexagonal SnS2 nanosheets onto electrospun TiO2 nanofibers: enhanced photocatalytic activity based on photoinduced interfacial charge transfer, Nanoscale 5 (2013) 606–618.
[27] Z.Y. Zhang, J.D. Huang, M.Y. Zhang, L. Yuan, B. Dong, Ultrathin hexagonal SnS2 nanosheets coupled with g-C3N4 nanosheets as 2D/2D heterojunction photocatalysts toward high photocatalytic activity, Appl. Catal. B Environ. 163 (2015) 298–305.
[28] K. Chang, Z. Wang, G.C. Huang, H. Li, W.X. Chen, J.Y. Lee, Few-layer SnS2/graphene hybrid with exceptional electrochemical performance as lithium-ion battery anode, J. Power Sources 201 (2012) 259–266.
[29] B. Luo, Y. Fang, B. Wang, J.S. Zhou, H.H. Song, L.J. Zhi, Two dimensional graphene-SnS2 hybrids with superior rate capability for lithium ion storage, Energy Environ. Sci. 5 (2012) 5226–5230.
[30] Y.C. Liu, H.Y. Kang, L.F. Jiao, C.C. Chen, K.Z. Cao, Y.J. Wang, H.T. Yuan, Exfoliated-SnS2 restacked on graphene as a high-capacity, high-rate, and long-cycle life anode for sodium ion batteries, Nanoscale 7 (2015) 1325–1332.
[31] Y.D. Zhang, P.Y. Zhu, L.L. Huang, J. Xie, S.C. Zhang, G.S. Cao, X.B. Zhao, Few-layered SnS2 on few-layered reduced graphene oxide as Na-ion battery anode with ultralong cycle life and superior rate capability, Adv. Funct. Mater. 25 (2015) 481–489.
[32] B.H. Qu, C.Z. Ma, G. Ji, C.H. Xu, J. Xu, Y.S. Meng, T.H. Wang, J.Y. Lee, Layered SnS2-reduced graphene oxide composite - a high-capacity, high-rate, and long-cycle life sodium-ion battery anode material, Adv. Mater. 26 (2014) 3854–3859.
[33] Y. Wu, P. Nie, L. Wu, H. Dou, X. Zhang, 2D MXene/SnS2 composites as high-performance anodes for sodium ion batteries, Chem. Eng. J. 334 (2018) 932–938.
[34] I. Calizo, A.A. Balandin, W. Bao, F. Miao, C.N. Lau, Temperature dependence of the Raman spectra of graphene and graphene multilayers, Nano Lett. 7 (2007) 2645–2649.
[35] L. Su, Y. Zhang, Y. Yu, L. Cao, Dependence of coupling of quasi 2-D MoS2 with substrates on substrate types, probed by temperature dependent Raman scattering, Nanoscale 6 (2014) 4920–4927.
[36] D. Yoon, Y.-W. Son, H. Cheong, Negative thermal expansion coefficient of graphene measured by Raman spectroscopy, Nano Lett. 11 (2011) 3227–3231.
[37] Z. Li, J. Wu, C. Wang, H. Zhang, W. Yu, Y. Lu, X. Liu, High-performance monolayer MoS2 photodetector enabled by oxide stress liner using scalable chemical vapor growth method, Nanophotonics (2020), https://doi.org/10.1515/nanoph-2019-0515.
[38] J.P. Perdew, K. Burke, M. Ernzerhof, Generalized gradient approximation made simple, Phys. Rev. Lett. 77 (1996) 3865–3868.
[39] P.E. Blöchl, Projector augmented-wave method, Phys. Rev. B 50 (1994) 17953–17979.
[40] H.J. Monkhorst, J.D. Pack, Special points for Brillouin-zone integrations, Phys. Rev. B 13 (1976) 5188–5192.
[41] P.S. Shternin, D.G. Yakovlev, Electron thermal conductivity owing to collisions between degenerate electrons, Phys. Rev. D 74 (2006), 043004.